PROCEEDINGS OF THE ROYAL SOCIETY A

Proc. R. Soc. A (2006) **462**, 2997–3026
doi:10.1098/rspa.2006.1703
Published online 2 May 2006

Dynamic sliding of frictionally held bimaterial interfaces subjected to impact shear loading

By G. Lykotrafitis and A. J. Rosakis*

Graduate Aeronautical Laboratories, California Institute of Technology, Pasadena, CA 91125, USA

The fast frictional sliding along an incoherent interface of a bimaterial system composed of a Homalite and a steel plate is studied experimentally in a microsecond time-scale. The plates are held together by a static uniform compressive pre-stress while dynamic sliding is initiated by asymmetric impact. The full-field technique of dynamic photoelasticity is simultaneously used with a local technique of velocimetry based on laser interferometry. In the case where the impact loading is applied to the Homalite plate, a shear Mach line originates from a disturbance propagating along the interface supersonically with respect to the dilatational wave speed of Homalite and it crosses the P-wave front. The sliding starts well behind the P-wave front in Homalite and it propagates with a supershear speed with respect to Homalite. A fast interface wave and a wrinkle-like opening pulse (detachment wave) travelling along the interface are observed. When the impact loading is applied to the steel plate, the local sliding velocity measurement reveals that sliding initiates with the arrival of the P-wave front in the steel plate.

Keywords: dynamic frictional sliding; incoherent interface; bimaterial system; photoelasticity; in-plane velocity measurement; wrinkle-like pulse

1. Introduction

Dynamic frictional sliding along incoherent interfaces between two deformable solids is of great interest to both engineering and applied sciences, since it appears in almost all physical phenomena, which involve interfaces. Examples include moving machinery surface interactions (relevant to both macro- and micro-machinery operations), material processing (e.g. cutting), bolted joints, sandwich structures, the failure of fibre reinforced composites (e.g. dynamic fibre pullout) as well as earthquake dynamics (fault rupture). Here, we confine our attention to dynamic sliding induced by impact shear loading.

The classical Amontons–Coulomb description of friction states that shear stress at an interface is proportional to the normal stress, with the coefficient of proportionality being the coefficient of friction (Persson 2000). In this classic description of friction, two coefficients of friction are identified: a static coefficient of friction that governs the onset of sliding and a dynamic coefficient of friction that characterizes the behaviour during sliding. In a slightly more advanced

* Author for correspondence (rosakis@aero.caltech.edu).

Received 16 December 2005
Accepted 28 February 2006

description, the coefficient of friction may take the form of a simple function of sliding distance (slip) or of sliding speed or of both while the linear dependence on normal stress is still preserved.

From the microscale point of view, an evolving population of contacts and their local deformation, phase transition and fracture and the presence of various lubricants appear to play an important role in controlling the functional form of the dependence of frictional strength on sliding speed and normal stress. From the phenomenological point of view, rate and state models of friction have recently been introduced in an attempt to replace the simplistic Amontons–Coulomb descriptions given above (e.g. Dieterich 1979; Rice & Ruina 1983; Ruina 1983; Linker & Dieterich 1992; Prakash & Clifton 1993; Prakash 1998). Such models, based on experimental observations, attempt to describe the local microprocesses of surface interaction and to introduce the notion of 'system memory' through appropriately chosen state variables. Rate and state models of friction have come to the fore because they substantially influence the predicted mode and stability of the dynamic interfacial sliding processes (Coker *et al.* 2005).

A central issue in the modelling of frictional sliding is the duration of the slip at a point on the interface compared to the duration of sliding. The most classic approach of sliding uses shear crack models (crack-like mode), where the slip duration at a point is a significant fraction of the overall sliding (Freund 1990). According to the pulse-like model, the duration of slip at a point is considerably shorter than the duration of sliding (Heaton 1990). In general, narrow slip pulses can be generated during dynamic sliding along interfaces by strongly velocity-weakening friction on a homogeneous system (same material across the interface; Rice 2001), by strong fault zone heterogeneities (Day 1982) or by variations in normal stress along the rupture interface. All of the above conditions (velocity weakening, heterogeneities and bimaterial contrast) can produce slip pulses with low dynamic stress at the active part of the slip and provide satisfactory solution to the heat flow paradox.

Renardy (1992) and Adams (1995) showed that sliding along a bimaterial interface governed by Amontons–Coulomb friction is unstable to periodic perturbations, with an instability growth rate proportional to the wave number, for a wide range of friction coefficients and material properties. Ranjith & Rice (2001) found that for moderate material contrast for which the generalized Rayleigh wave exists, there are unstable modes for all values of the Coulomb friction coefficient. On the other hand, when the material contrast is large enough so that the generalized Rayleigh wave does not exist, such unstable modes appear only for a friction coefficient larger than a critical value. For lower values of friction coefficient, periodic disturbances are either neutrally stable (do not grow with time) or stable (diminishing with time giving rise to stable sliding). Mathematically, instability makes the response of a material interface with Coulomb friction ill-posed (no solution exists) to generic (non-periodic) perturbations or pulses, which can be thought of as infinite superposition of periodic perturbations of various wavelengths. Physically, the above instability implies that during sliding, energy is transferred to shorter wavelengths, leading to pulse sharpening and splitting. Numerically, the splitting of individual pulses creates inherent grid-size dependency for numerical calculations (Andrews & Ben-Zion 1997; Ben-Zion & Andrews 1998). Ranjith & Rice (2001) demonstrated

that an experimentally based rate and state dependent friction law (Prakash & Clifton 1993; Prakash 1998), in which the shear strength in response to an abrupt change in normal stress evolves continuously over time, provides well-posedness (regularization) to the problem of generic perturbations propagation (solutions for non-splitting single pulses can be found). Convergence through grid size reduction is then achieved (Cochard & Rice 2000). We also note that Harris & Day (1997, 2005) had a different approach for dealing with this challenge of numerical stability by introducing system viscosity.

Classic dynamic fracture theories (Freund 1990; Broberg 1999) of shear cracks propagation have many similarities to the frictional process. However, unlike the case of coherent interfaces, where the resistance to failure through sliding comes from the bond between the plates, in the case of incoherent interfaces the resistance to sliding comes from the frictional forces between the surfaces in contact. The issue of limiting propagation speeds arises in the dynamic fracture mechanics of growing shear cracks (Andrews 1976; Day 1982; Archuletta 1984; Freund 1990; Broberg 1999; Rosakis 2002). These theories treat the rupture front as a distinct point (sharp-tip crack). The crack-like rupture of coherent interfaces, separated by similar and dissimilar solids subjected to dynamic shear loading, has been the subject of extensive experimental, numerical and analytical investigations in the past years and has been summarized by Rosakis (2002). Of relevance to the present study is the persistent occurrence of intersonic shear rupture along coherent bimaterial interfaces. The first experimental observations of intersonically travelling cracks were made in connection with crack propagation along the interface of bimaterial systems (Tippur & Rosakis 1991; Liu *et al.* 1993; Lambros & Rosakis 1995; Singh & Shukla 1996; Kavaturu *et al.* 1998; Rosakis *et al.* 1998). It has been numerically modelled by Coker *et al.* (2003) using the cohesive element methodology. We finally mention that supershear rupture in bimaterial systems is also reported in Harris & Day (1997).

The possibility of generating wrinkle-like pulses in incoherent frictionless contact between two dissimilar solids, when separation does not occur, was first investigated by Achenbach & Epstein (1967). These 'smooth contact Stonely waves' (also known as slip waves or generalized Rayleigh waves) are qualitatively similar to those of bonded contact (Stonely waves) and occur for a wider range of material combinations. Comninou & Dundurs (1977) found that self-sustained slip waves with interface separation (detachment waves or wrinkle-like slip pulses) can propagate along the interface of two similar or different solids, which are pressed together. The constant propagation speed of these waves was found to be between the Rayleigh wave speed and the shear wave speed of the slowest material. Weertman (1980) obtained a two-dimensional self-sustained wrinkle-like slip pulse propagating at the generalized Rayleigh wave speed along a bimaterial interface governed by Coulomb friction when the remote shear stress was less than the frictional strength of the interface. Finite-difference calculations of Andrews & Ben-Zion (1997) show the propagation of wrinkle-like pulses along a bimaterial interface governed by Coulomb friction. Particle displacement in a direction perpendicular to the fault is much greater in the slower material than in the faster material, resulting in a separation of the interface during the passage of the slip pulse. The recent paper by Andrews & Harris (2005) is also a very important reference reflecting the on-going discussion

on this subject. Anooshehpoor & Brune (1999) discovered such waves in rubber sliding experiments (using a bimaterial system consisting of two rubber blocks with different wave speeds). The above-mentioned detachment waves are radically different from the Schallamach waves (Schallamach 1971), which propagate very slowly compared to the wave speeds of the solid.

In this paper, the fast frictional sliding along an incoherent interface of a bimaterial system composed of a Homalite and a steel plate is studied experimentally in a microsecond time-scale. The plates are held together by a static uniform compressive pre-stress while dynamic sliding is initiated by asymmetric impact. The technique of dynamic photoelasticity in conjunction with high-speed photography is used to record the evolution of the maximum shear stress contours along the interface and in the bulk. In addition to photoelasticity, a laser interferometry-based technique is employed to measure locally the sliding velocity at a point at the interface. The simultaneous use of the full-field technique of photoelasticity and the local technique of velocimetry is proven to be a very powerful tool in the investigation of dynamic sliding.

The response of the Homalite-steel bimaterial system differs according to whether the impact loading is applied to the Homalite plate or to the steel plate. In the first case, the interaction between the impact wave and the pre-existing static field causes the generation of a relatively broad eye-like fringe formation emanating from the interface behind the P-wave front. A disturbance travelling at the interface at a constant speed close to the Rayleigh wave speed of steel, which is higher than the P-wave speed of Homalite, generates a shear Mach line crossing the P-wave front and the eye-like fringe structure. Velocimetry reveals that sliding initiates behind the eye-like fringe pattern. A second shear Mach line, originating from the sliding tip, appears in the photoelastic images, indicating that the sliding is supershear with respect to the shear wave speed of Homalite. A fast interface wave appears in the cases of high-impact speeds and low pre-stress. It propagates at a constant speed between the shear wave speed and the P-wave speed of Homalite. A self-sustaining wrinkle-like opening pulse, propagating along the bimaterial interface at a constant speed between the Rayleigh wave and the shear wave speed of Homalite, is also observed. When the impact load is applied to steel plate, then the data acquired by the velocimeter are the only useful source of information. Analysis of these data shows that sliding at a given point initiates with the arrival of the P-wave front there. In both cases, sliding always occurs in a crack-like mode.

This work contributes significantly in the research of dynamic frictional sliding because it elucidates in unprecedented detail how dynamic frictional sliding, induced by impact loading, occurs in bimaterials systems. It also demonstrates for the first time the physical attainability of the theoretically predicted wrinkle-like sliding modes. The results obtained in this work cannot be directly used to validate the various friction laws, since there is no appropriate theoretical solution for the experimental configuration employed here. However, the velocity measurements along with the recorded evolution of the patterns of maximum shear stress contours can be indirectly used to validate the theoretical models of friction through numerical simulations. Finite element calculations can be performed to verify or discard various types of friction laws on the basis of agreement or essential disagreement between the numerical and the experimental results.

2. Materials and specimen configuration

Experiments were performed to investigate the nature of dynamic frictional sliding along the incoherent interface of a high-contrast bimaterial system. The bimaterial specimen consisted of a Homalite-100 plate and a steel plate held together by a uniform compressive stress (see figure 1). Homalite-100 is a mildly rate-sensitive brittle polyester resin that exhibits stress-induced birefringence with an optical coefficient of $F_\sigma = 22.6\ \mathrm{kN\ m^{-1}}$. At the strain rate developed during the experiments (in the order of $10^3\ \mathrm{s^{-1}}$) and at room temperature, Homalite exhibits a purely linear elastic behaviour. The density of Homalite is $1230\ \mathrm{kg\ m^{-3}}$. The dilatational, shear and Rayleigh wave speeds in Homalite are $C_1^{\mathrm{H}} = 2583\ \mathrm{m\ s^{-1}}$, $C_2^{\mathrm{H}} = 1249\ \mathrm{m\ s^{-1}}$ and $C_{\mathrm{R}}^{\mathrm{H}} = 1155\ \mathrm{m\ s^{-1}}$, respectively. Steel was chosen as the other half of the bimaterial system because it provides a strong material property mismatch across the interface, similar to mismatches encountered in composites. The density of steel is $7830\ \mathrm{kg\ m^{-3}}$. The dilatational, shear and Rayleigh wave speeds in steel are $C_1^{\mathrm{S}} = 5838\ \mathrm{m\ s^{-1}}$, $C_2^{\mathrm{S}} = 3227\ \mathrm{m\ s^{-1}}$ and $C_{\mathrm{R}}^{\mathrm{S}} = 2983\ \mathrm{m\ s^{-1}}$, respectively. The wave speeds for Homalite and steel were obtained by ultrasonic measurements using shear and pressure transducers operating at 5 MHz.

In the experiments, the configuration was approximated by plane stress conditions, since plate specimens 76.2 mm high, 139.7 mm long and 9.525 mm thick were employed. The shear wave speeds are identical in three-dimensions and for the plane stress approximation. The same is true for the Rayleigh wave speed, since the contribution in the Rayleigh wave formation comes primarily from the shear wave. However, the plane stress dilatational wave speeds of Homalite-100 and steel are $C_{1\sigma}^{\mathrm{H}} = 2187\ \mathrm{m\ s^{-1}}$, $C_{1\sigma}^{\mathrm{S}} = 5378\ \mathrm{m\ s^{-1}}$, respectively.

3. Experimental set-up and procedure

A combination of two experimental techniques was used in this investigation. Dynamic photoelasticity, which gives the full field maximum shear stress distribution, was used in conjunction with a new technique based on laser interferometry. This technique provides a continuous local measurement of the in-plane horizontal and vertical components of the relative velocity of two adjacent points across the bimaterial interface. The initiation and evolution of sliding was explored through photoelasticity and velocimetry at a micro-second time-scale.

The compressive stress was applied with a hydraulic press calibrated using a load cell. The asymmetric impact loading was imposed via a cylindrical steel projectile with a diameter of 25 mm and a length of 51 mm, fired by a gas gun. A steel buffer 73 mm high, 25.4 mm long and 9.525 mm thick was attached to the impact side of the Homalite plate to prevent shattering and to induce a more or less planar loading wave.

(*a*) *Dynamic photoelasticity set-up*

A typical experimental set-up for dynamic photoelasticity experiments is shown in figure 2. The optical set-up was arranged for a light field. Isochromatic fringes are contours of maximum in-plane shear stress $\tau_{\max}$ governed by

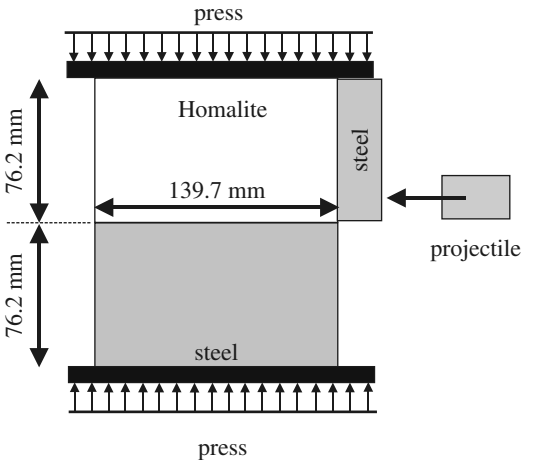

Figure 1. Geometry and loading configuration for a bimaterial specimen consisting of a Homalite and a steel plate.

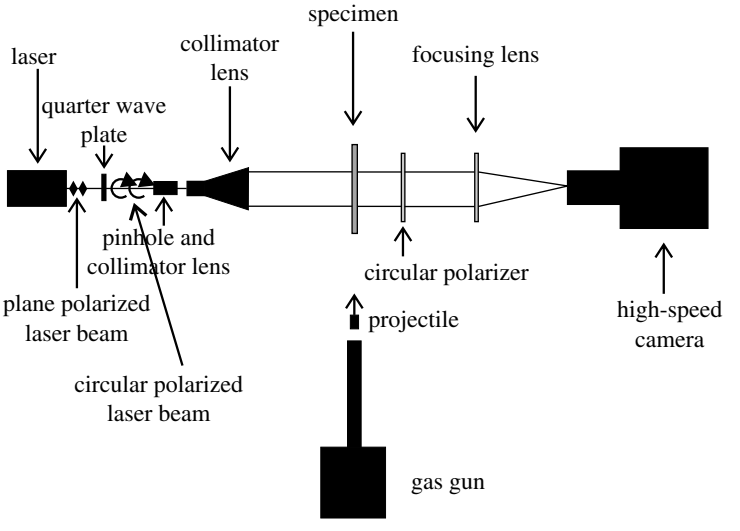

Figure 2. Dynamic photoelasticity set-up. A circular polarized laser beam passes through the specimen that is subjected to uniform confining stress and to impact shear loading via a projectile fired by a gas gun. The resulting isochromatic fringe patterns are recorded by a high-speed digital camera.

the stress optical law

$$2\tau_{\max} = \sigma_1 - \sigma_2 = NF_\sigma/h,$$

where F_σ is the material's stress optical coefficient, h is the specimen thickness, σ_1, σ_2 are the principal stresses and $N = n + 1/2$ (with $n = 0, 1, 2, \ldots$) is the isochromatic fringe order. A continuous laser was used as the light source in our experiments. The vertically polarized laser beam first passed through a quarter wave plate, which transformed it into a circular polarized beam. Then it

expanded in a uniform laser beam of 130 mm diameter. The laser beam was transmitted through the specimen and an analyser. The resulting photoelastic fringe pattern was recorded with a high-speed digital camera (Cordin model 220), which is able to record 16 distinct frames at framing rates up to 100 million frames per second. In this experimental work, most of the high-speed photography was performed at 250 000–1 000 000 frames per second. It is noted that the field of view was wide enough to cover most of the specimen.

(*b*) *Sliding velocity measurement set-up*

The local sliding velocity was obtained as follows. A pair of fibre-optic velocimeters measured the horizontal particle velocities at two adjacent points across the interface. The horizontal relative velocity history was obtained by subtracting the velocity of a point on the lower plate from the velocity of a point across the interface on the upper plate. A schematic representation of the set-up is shown in figure 3*a*. The laser beams emitted from the velocimeters were focused on points M_1 and M_2 on the thin vertical surfaces of the reflective membranes, which were attached to the surfaces of the Homalite (top) and steel (bottom) plates, respectively. The distance of each point from the interface was less than 250 μm before compression, and both points had the same horizontal distance from the impact side of the Homalite plates. A picture of the actual set-up is presented in figure 3*b*. The technique is presented in detail in Lykotrafitis *et al.* (2006).

(*c*) *Simultaneous measurement of the horizontal and vertical components of the velocity*

The two velocimeters can be used to measure not only the horizontal component of the in-plane velocity, but also the vertical component. For this, the laser beam is aimed perpendicular to the narrow horizontal surface of the reflective membrane. Preliminary experimental results showed that the velocities in steel plate are one order of magnitude slower than the velocities in Homalite plate. Taking advantage of this fact, we assumed that particle velocities in the steel were negligible and we carried out several tests using the two velocimeters we had at our disposal to record both the horizontal and vertical in-plane particle velocities. These were subsequently interpreted as sliding and opening speeds, respectively. A schematic of the set-up employed for the measurement is shown in figure 4.

4. Sliding induced by an impact shear loading applied on the Homalite plate of a bimaterial specimen

(*a*) *Initiation and evolution of dynamic frictional sliding*

In the present experiments, dynamic photoelasticity (in conjunction with high-speed photography) was combined with velocimetry to investigate the initiation and evolution of frictional sliding along the incoherent interface of a bimaterial specimen consisting of Homalite and steel. The specimen was subjected to a uniform compressive load of 10 MPa and impacted on the Homalite side at a speed of 16.5 m s^{-1}. The sequence of photoelastic images in figure 5 is studied in

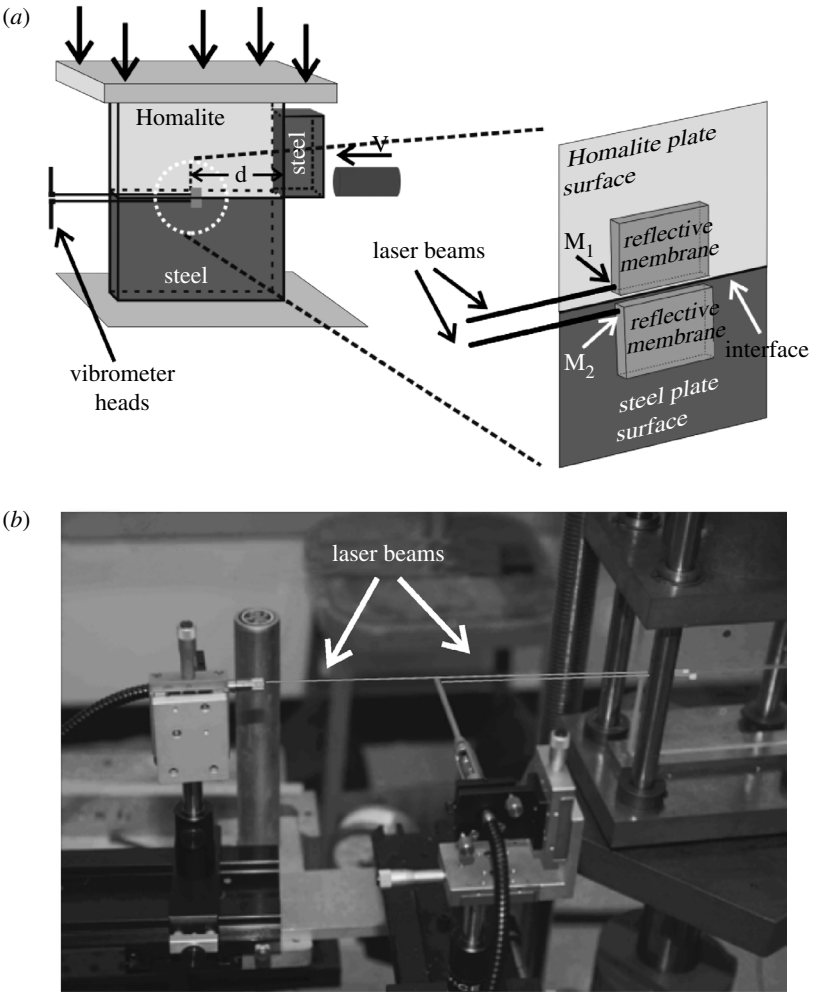

Figure 3. (*a*) Schematic illustration of the experimental configuration for the sliding velocity measurement. The area inside the dotted line is shown magnified. Points M_1 and M_2 were at the same distance d from the impact side of the Homalite plate. (*b*) Photograph of the actual set-up.

combination with the horizontal velocities measurements presented in figure 6. The images in figure 5 show the isochromatic fringe pattern in the Homalite plate at selected times. A pair of fibre-optic velocimeters recorded the history of the horizontal in-plane velocities of two adjacent points, M_1 and M_2 in the Homalite (top) and steel (bottom) plate, respectively (see figure 3). Both points were at the same horizontal distance of 110 mm from the impact side of the Homalite plate and at less than 250 μm from the interface. Figure 6 shows the histories of the horizontal in-plane velocities of both points, as well as the history of the relative horizontal velocity. The insert in figure 6*a* displays the history of the relative displacement, which was obtained from the velocity history by numerical integration.

The images in figure 5*a–e* have similar structure. At 110 μs (see figure 5*f*), reflected waves from the free left side of the plate had entered the picture

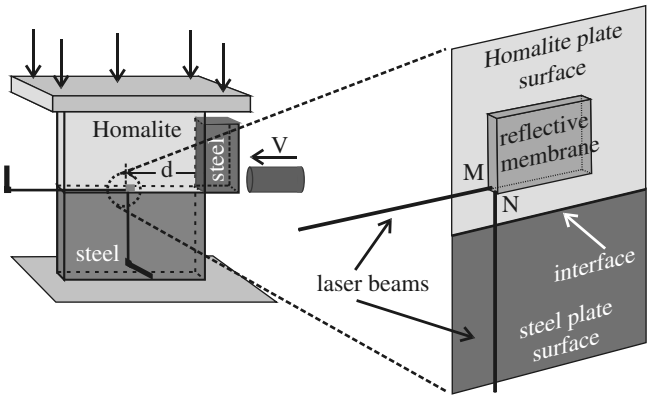

Figure 4. Schematic illustration of the experimental configuration for the simultaneous measurement of the horizontal and vertical components of the particle velocity. The area inside the dotted line is shown magnified.

and the sliding process became transient, resulting in a distorted photoelastic fringe pattern. As can be seen in figure 5*a*, the compressive stress wave (P-wave) in the Homalite plate arrives from the right, in front of a relatively broad fringe structure (shown just behind point F), which has a rib-eye structure and emanates from the interface. Since this structure was missing in similar experiments, without external pressure, we can safely conjecture that it was caused by the interference of the impact wave with the pre-existing static pressure.

A head wave emanates from point A on the interface and crosses the eye-like fringe structure. Point A is ahead of the P-wave front in the Homalite plate. This shows that a disturbance was travelling along the interface at a speed higher than the P-wave in Homalite. The propagation speed V of the disturbance was determined in each frame by measuring the Mach angle θ and using the relation $V = C_2^{\mathrm{H}}/\sin\theta$, where C_2^{H} is the shear wave speed of Homalite. The average value was $2830\ \mathrm{m\ s^{-1}} = 0.88\,C_2^{\mathrm{S}} = 0.95\,C_{\mathrm{R}}^{\mathrm{S}} = 1.3\,C_{1\sigma}^{\mathrm{H}} = 1.1\,C_1^{\mathrm{H}}$, where C_2^{S} is the shear wave speed of steel, $C_{\mathrm{R}}^{\mathrm{S}}$ is the Rayleigh wave speed of steel, $C_{1\sigma}^{\mathrm{H}}$ is the plane stress P-wave speed of Homalite and C_1^{H} is the plane strain P-wave speed of Homalite. The disturbance travelled at a speed 5% lower than the Rayleigh wave speed of steel and 12% lower than the shear wave speed of steel. This result was consistently repeatable. We note that this disturbance is not a generalized Rayleigh wave, since such waves do not exist for bimaterial systems with large contrast in material properties, such as we have in this case (Achenbach & Epstein 1967; Ranjith & Rice 2001; Rice *et al.* 2001). The photoelastic images do not provide conclusive evidence regarding the exact nature of the disturbance at point A.

The effect of the above disturbance on the process of sliding was deciphered by using the recorded velocity data presented in figure 6*b*, which shows an expanded view of the history of the velocity of points M_1 and M_2 at the initiation of sliding. Point M_2, which was on the surface of the steel plate, started moving first at approximately 57.5 μs, under the influence of the compressive stress wave propagating in the steel plate. Point M_1 on the Homalite plate started moving at

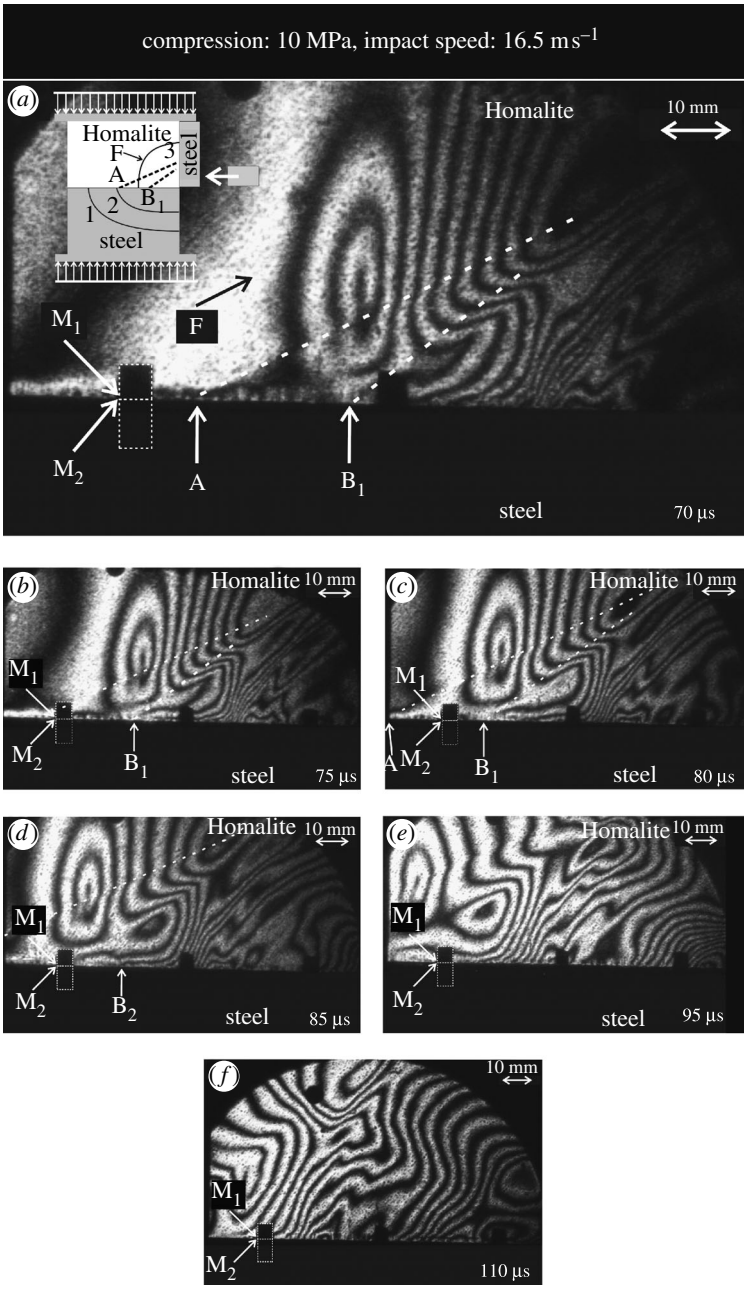

Figure 5. A sequence of isochromatic fringe patterns showing an intersonic frictional sliding, the corresponding shear Mach line (B_1) and a shear head wave (A). M_1 and M_2 are the positions of the velocity measurements.

59 μs. During the following 14 μs, M_1 and M_2 were moving at the same speed until approximately 72 μs. At that time, the point in the steel plate (M_2) decelerated and its velocity became negative. The velocity of the point on the Homalite plate (M_1) followed the same trend after approximately 1.5 μs. Up to

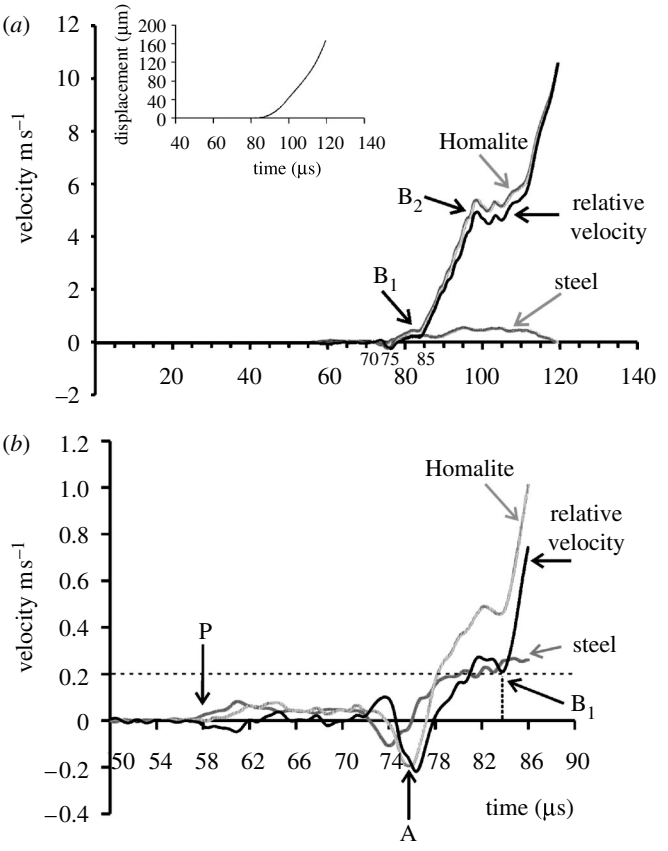

Figure 6. (*a*) Histories of the horizontal in-plane velocities and of the relative velocity, measured at two adjacent points across the interface, 110 mm from the impact side of the Homalite plate. The sliding initiated at B_1. The insert shows the history of the relative displacement. (*b*) Detail of the velocity history diagram, showing the arrival of the P-wave front in the steel plate (P), the arrival of the shear wave front in the steel plate (A) and the sliding initiation (B_1).

that time, there was no sliding, since both points travelled together under the influence of the P-wave in the steel plate, and the relative velocity oscillated around zero. Then, at about 74 and 76 μs, respectively, the velocities of M_1 and M_2 started increasing again. However, in this case, the velocity of the point on the Homalite surface increased faster than the velocity of the point on the steel plate. The corresponding photoelastic frame taken at 75 μs (figure 5*b*) shows that a Mach line emanated from the interface, at a short distance in front of the reflective point, and ahead of the P-wave front in the Homalite plate. A very simple calculation shows that a disturbance travelling at a speed of $0.95C_{\mathrm{R}}^{\mathrm{S}} = 1.3C_{1\sigma}^{\mathrm{H}} = 1.1C_{1}^{\mathrm{H}}$ is expected to be at the reflective point at about 74 μs. This confirms that the disturbance caused the increase of the particle velocities. The disturbance was supersonic with respect to Homalite, and therefore, it was ahead of the P-wave front travelling in the Homalite plate. In addition, a Mach cone was formed with a tip at the disturbance. The initial impact of the projectile on the steel buffer created a compression P-wave, transmitted into the Homalite plate. Because of friction, some of the energy also

transmitted into the steel plate. The P-wave travelled faster in the steel plate than in the Homalite plate, and thus, a precursor effect emerged. Nevertheless, photoelasticity is not very sensitive to compression, and because of this, we could not see a possible Mach cone associated with the interface disturbance travelling at the P-wave speed of steel. The disturbance, however, caused the photoelastic fringe pattern to warp enough for it to be captured by the high-speed camera. The insert in figure 5*a* schematically illustrates the loading configuration, the resulting wave fronts, the shear head wave and the supershear sliding tip with the resulting Mach cone. Curves 1–3 correspond to the P-wave front in the steel plate, the shear wave front in the steel plate and the P-wave front in the Homalite plate. Point A represents the disturbance, just behind the shear wave front in the steel plate, and point B_1 represents the sliding tip.

In figure 5*c*, the tip of the first Mach line has passed the position of velocity measurement, whereas the eye-like structure has just arrived there. The velocimeter recording shows that at approximately 76 μs the relative horizontal velocity between M_1 and M_2 has increased, but yet not very sharply. We also note that the numerically calculated relative horizontal displacement between the points M_1 and M_2 was less than 1 μm until 84 μs. This indicates that until 84 μs there was no sliding, but only shear elastic deformation of the material close to the interface (material between M_1 and M_2). Thus, the disturbance and the eye-like fringe structure did not create slip.

However, at approximately 84 μs, a drastic change occurred in the relative velocity and in the relative displacement (see figure 6*a*). The velocity of the measurement point in the Homalite plate increased rapidly, whereas the velocity of the point in the steel plate remained almost constant. This resulted in a very steep rise in the relative velocity and in a very abrupt change in the slope of the relative displacement versus time diagram. We conclude that the sliding, at the position of measurement, started at around 84 μs. The corresponding photoelastic frame (see figure 5*d*) captured at 85 μs is extremely revealing, in which a fringe concentration point (point B_1 of figure 5*a*,*b*) coincides with the measurement position. It is the sliding tip, and because it propagated with a supershear speed, a Mach line emanated from this position. Indeed, following the positions of the tip in different frames and using a linear interpolation, we obtained the tip propagation velocity, which was $1970\ \mathrm{m\ s^{-1}} = 1.58 C_2^{\mathrm{H}}$, higher than the shear wave speed of Homalite.

The velocimeter measurement (figure 6*a*) shows that the speed increased sharply from 84 to approximately 98 μs, and then it remained almost constant until 110 μs, where a second acceleration event occurred. The time instance of 98 μs (when the acceleration ceased) corresponded to a fringe concentration point B_2 (see figure 5*d*). After point B_2, the fringes were parallel to the interface, which means that a constant maximum shear stress field was formed. In figure 5*f*, captured at 110 μs, the area of the photoelastic pattern with inclined fringes arrived at the measurement position, and this coincided with the initiation of the secondary acceleration caused by the arrival of the reflected waves from the free side of the Homalite plate. From the relative velocity history diagram, we conclude that sliding was continuous during the recording time. This means that sliding occurred in a crack-like mode.

The above exhaustive study of the experimental results clearly shows the power of the proposed point velocity measurement in combination with the full

field technique of photoelasticity. We were able to completely identify the different fringe formations in the photoelastic images and explicitly connect them to the changes in sliding velocity. We finally note that, after the initiation of sliding, the in-plane horizontal particle velocity in the steel plate was one order of magnitude lower than the velocity in the Homalite plate. This is true not only for the experiment analysed above but for all of the performed experiments using Homalite-steel bimaterial specimens, impacted on the Homalite plate.

The findings of this experiment are similar to results obtained by experiments on crack growth in bimaterials (Samudrala *et al.* 2002; Samudrala & Rosakis 2003; Coker *et al.* 2003). The first experimental observations of intersonically travelling cracks were made in connection with crack propagation along the interface of bimaterial systems (Tippur & Rosakis 1991; Liu *et al.* 1993; Lambros & Rosakis 1995; Singh & Shukla 1996; Kavaturu *et al.* 1998; Rosakis *et al.* 1998). In the shear crack propagation experiments, the Homalite and steel plates were bonded together and a notch was machined along the bond line at one edge. Thus, the resistance to rupture was generated mainly from the bond. In the present study, the resistance to sliding was due to the frictional stress between the surfaces of the two plates in contact. It is noted that the frictional resistance was not uniform along the interface and not constant with time, since the dynamic compression and the sliding velocity were changing with position and time.

(*b*) *Influence of impact speed and confining stress on sliding*

Figure 7*a* displays an instantaneous isochromatic fringe pattern developed in an experiment, where the impact speed decreased to 12 m s^{-1} while the confining pressure was kept constant at 10 MPa. The fringe configuration has basically the same structure as that in the experiment presented in the previous section. A head wave which crosses the eye-like fringe structure appears as, does the fringe formation B_1B_2. The recorded velocity history of points M_1 and M_2 is illustrated in figure 7*b*. In this case, however, the velocities were measured 70 mm from the impact side of the Homalite plate and the maximum speed was less than 10 m s^{-1}, which is the velocimeter limit. We thus captured the evolution of the velocities over a longer period of time than before. By synchronizing the velocity history recordings in figure 7*a* with the captured high-speed images, the different features appearing in the photoelastic image can be identified.

The initial disturbance (at point A), which travelled at approximately 2955 m s^{-1} $= 1.14C_1^{\mathrm{H}} = 2.37C_2^{\mathrm{H}} = 0.92C_2^{\mathrm{S}}$ and created the head wave, which crossed the eye-like fringe structure, arrived at the measurement position at 96 μs. The sliding started at point B_1 at approximately 103 μs and was propagating at a supershear speed of 2097 m s^{-1} $= 1.68C_2^{\mathrm{H}}$. At approximately 110 μs the velocity started increasing faster; this is shown in the photoelastic picture as a disturbance in the fringe structure (second dotted line emanating from point G at the interface). At approximately 112 μs, when point B_2 arrived at the measurement position, the velocity slowed down, and was oscillating until 120 μs, when another acceleration occurred. Then, the velocity remained high at approximately 6 m s^{-1} for 30 μs. The velocity then decreased until approximately 180 μs, when another acceleration started, caused by the arrival of the reflected waves from the free left side of the Homalite plate. The last acceleration

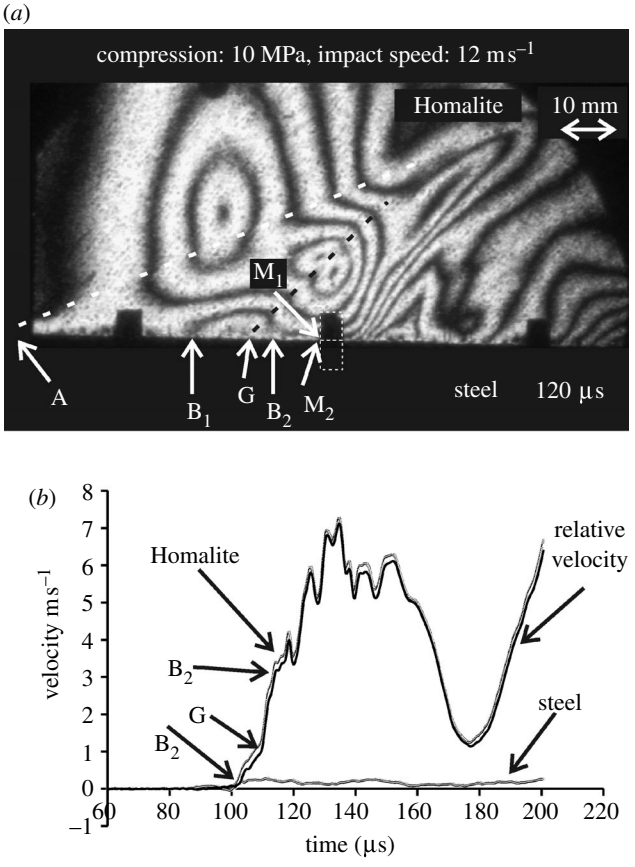

Figure 7. (*a*, *b*) Representative isochromatic fringe pattern and corresponding horizontal velocity histories and relative horizontal velocity history of points M_1 and M_2 located 70 mm from the impact side of the Homalite plate. The head wave is highlighted by the white dotted line. The sliding started at B_1. The black dotted line marks the warping of the fringes related to a change in the slope of the horizontal particle velocity in Homalite, which occurred at 110 μs after impact.

in figure 6*a* happened sooner because the measurement point was closer to the free side of the Homalite plate, and the reflected waves arrived earlier in that case than here. The velocity of point M_2 on the steel plate was one order of magnitude lower than the velocity of point M_1, and thus, the relative velocity was almost identical with the velocity of point M_1.

Figure 8*a* shows the in-plane relative horizontal velocity history measured at the same distance of 70 mm from the impact side of the Homalite plate in two different experiments. The external compression was 10 MPa and the impact speeds were 13 and 12 m s^{-1}. The two measurements were consistent. They include an initial acceleration period and a period where the variation in speed is small. The relative velocity generated by the impact at 13 m s^{-1} was slightly higher than the sliding velocity generated from the impact at 12 m s^{-1} during the whole recording period. The duration of the first period of sliding was approximately 70 μs, the same for both experiments, and then a second period of sliding started because of the reflected waves from the free left side of the

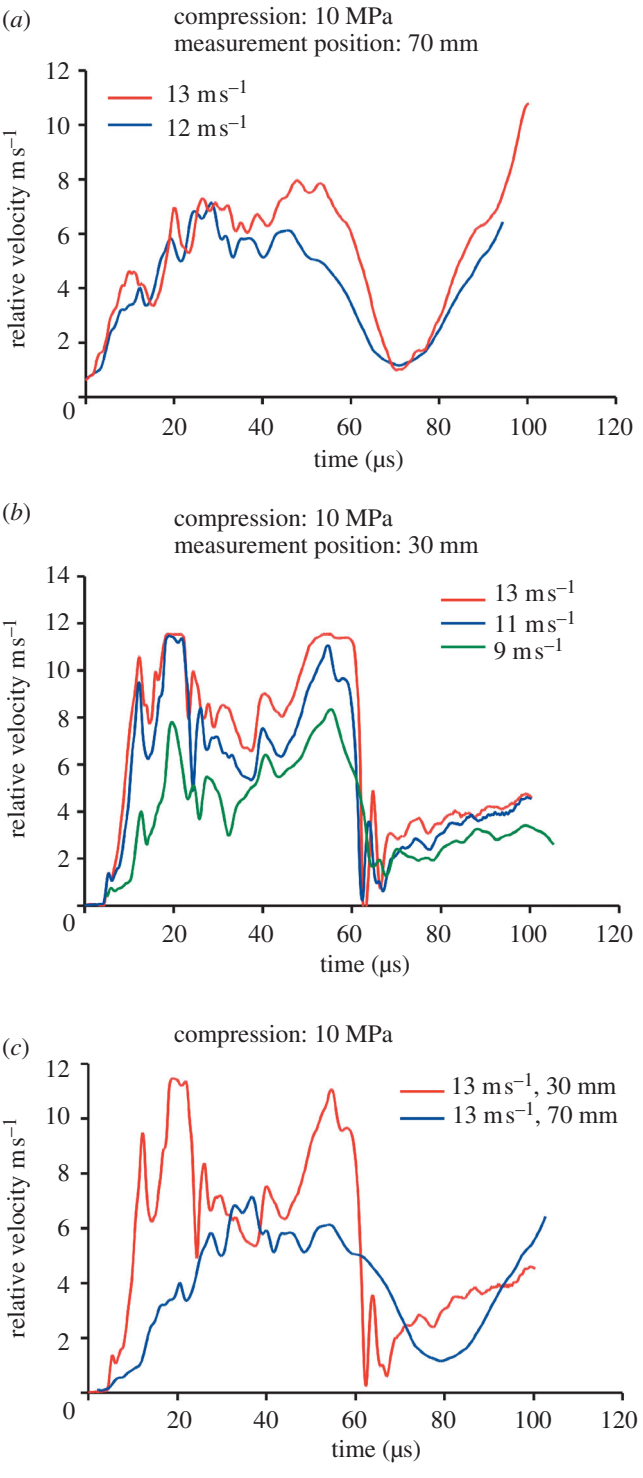

Figure 8. (*Caption overleaf.*)

Figure 8. (*Overleaf.*) (*a*) Comparison of the horizontal in-plane relative velocity histories of points M_1 and M_2, located at distances of 70 mm from the impact side of the Homalite plate, for different impact speeds. (*b*) Comparison of the horizontal in-plane relative velocity histories of points M_1 and M_2, located at distances of 30 mm from the impact side of the Homalite plate, for different impact speeds. (*c*) Comparison of the horizontal in-plane relative velocity histories of points M_1 and M_2, located at distances of 70 and 30 mm from the impact side of the Homalite plate, for the same impact speed of 13 m s^{-1}. In all cases, the external compression is 10 MPa.

Homalite plate. The in-plane relative horizontal velocities measured 30 mm from the impact side of the Homalite plate are displayed in figure 8*b*, for three different experiments performed at 10 MPa external confining pressure and at impact speeds of 9, 11 and 13 m s^{-1}. The duration of the first period of sliding was approximately 60 μs, the same for all three cases. The relative velocities increased with the impact speed. We mention that the velocity corresponding to an impact speed of 13 m s^{-1} saturated the velocimeter at around 20 and 50 μs, but each time it recovered its measurement ability. It is also noted that the speeds after 70 μs increased slowly, because the reflected waves had not arrived at the measurement position before the end of the recording. In figure 8*c*, the horizontal velocity histories recorded 30 and 70 mm from the impact side of the Homalite plate are compared. In both cases, the impact speed was 13 m s^{-1}. The results show that the maximum velocity decreases because of attenuation. They also show that the duration of the initial period of sliding increases as the distance between the measurement position and the impact side of the Homalite plate increases.

In this paragraph, results are presented for confining stresses less than 10 MPa. In figure 9*a*, the confining stress was 5 MPa and the impact speed was 13 m s^{-1}. As the confining stress decreases, the eye-like fringe structure becomes less pronounced. By synchronizing the photoelastic images with the recorded relative velocity history (figure 9*b*), we can conclude that the sliding at the velocity measurement point M started at approximately 50 μs, when point B crossed the measurement position. The sliding speed was supershear ($1932\ \mathrm{m\ s^{-1}} = 1.55\,C_2^{\mathrm{H}} = 0.75\,C_1^{\mathrm{H}}$) and because of this a Mach line, highlighted by a dotted line, emanates from point B. A fringe structure can be seen at point C. It is noted that this structure crossed the measurement position at approximately 70 μs and it did not generate any visible effect on the velocity history diagram. It travelled at a speed of $1261\ \mathrm{m\ s^{-1}} = 1.0\,C_2^{\mathrm{H}}$, close to the shear wave speed of Homalite, and its character will be revealed in §4*c*. Decreasing the compression further at 1.5 MPa and keeping the impact speed at 13.5 m s^{-1}, the eye-like fringe structure has almost completely disappeared (see figure 9*c*). The fringe density is low and there is no visible discontinuity that would signify the initiation of sliding. However, by matching the velocity history diagram (figure 9*d*) with the sequence of the recorded photoelastic images, the sliding tip can be located at point B (figure 9*c*). The sliding at point M started at approximately 82 μs. At point C, a fringe structure appears travelling along the interface. Figure 9*b*,*d* show that the velocity of sliding increased more abruptly at lower compression than in the case of a confining stress of 10 MPa. This fact indicates that minor elastic effects took place before the initiation of sliding.

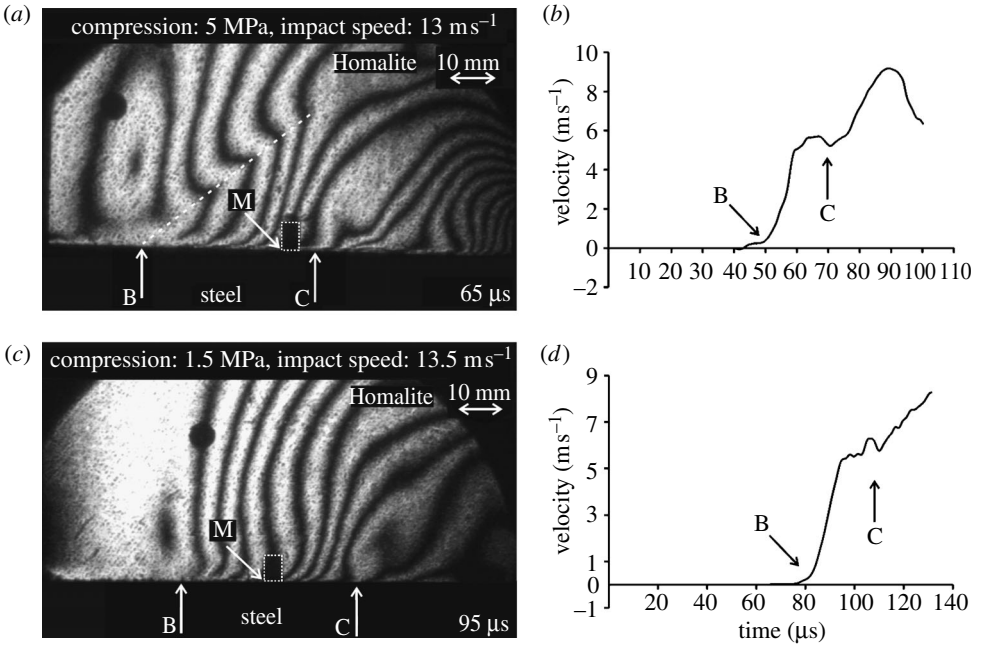

Figure 9. (*a*, *c*) Isochromatic fringe pattern captured during two different experiments. The supershear sliding initiated at B, whereas the wrinkle-like pulse is located at C. The dotted line highlights the Mach line. (*b*, *d*) Histories of the horizontal components of the in-plane particle velocity measured on the Homalite plate, 70 mm from its impact side.

(*c*) *Observation of wrinkle-like opening pulses*

The particle velocities in the steel plate were one order of magnitude less than the velocities in Homalite plate. Taking advantage of this fact, we used two velocimeters to record both the horizontal and vertical in-plane components of the velocity at a point on the Homalite plate, very close to the interface (see figure 4). We then interpreted our measurements as 'sliding' and 'opening' speeds by assuming that the steel plate was effectively rigid compared to the Homalite.

Figure 10 shows a sequence of six isochromatic patterns displaying the evolution of maximum shear stress contours in the Homalite plate. The confining external stress applied to the bimaterial specimen was 5 MPa and the speed of the projectile at impact was $22\ \mathrm{m\,s^{-1}}$. Figure 11*a* shows the histories of the horizontal and vertical in-plane components of the velocity at points M and N, respectively, on the Homalite plate. These points were at a distance of 70 mm from the impact side of the Homalite plate and at a distance of less than 250 μm from the interface (see figure 4). At 40 μs, the arrival of the P-wave front and the eye-like fringe structure at point M was captured by the high-speed camera (see figure 10*a*). This was fortuitous, because we could now combine visual evidence from the photoelastic picture with the recording of the velocimeters. Figure 11*a* shows that at 40 μs the horizontal velocity increased, whereas the vertical velocity became negative, showing that point N moved downward, towards the velocimeter head. The interpretation is clear. Point M moved to the left under the influence of the horizontal compressive stress generated by the impact.

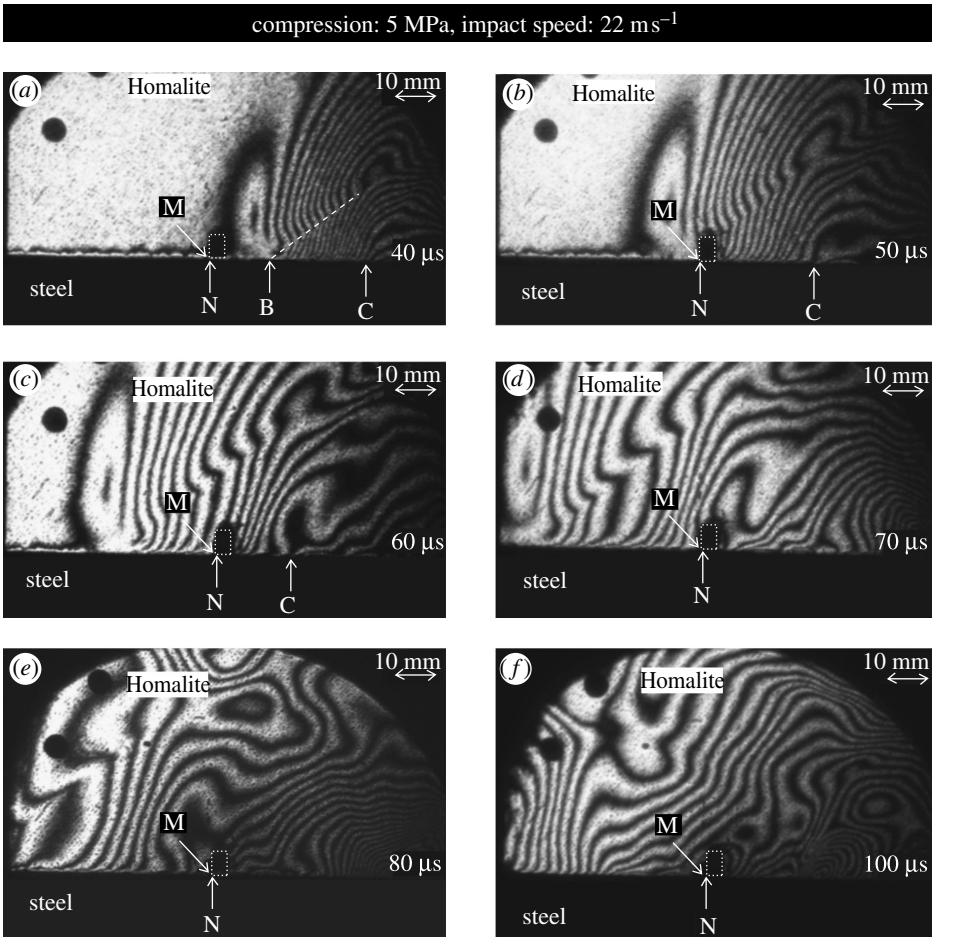

Figure 10. Sequence of isochromatic fringe patterns showing intersonic frictional sliding, the corresponding shear Mach line (B) and the wrinkle-like pulse (C). M and N are at the corner of the reflective membrane, where the horizontal and vertical in-plane components of the velocity were measured.

Because of the Poisson effect, the horizontal compressive stress induced a dynamic (inertial) vertical compressive stress that forced point N to move downward. Using the experience accumulated from the previous experiments, we estimated that sliding started at approximately 46 µs, when the relative velocity increased rapidly. From 40 to 46 µs, elastic shearing occurred, whereas sliding initiated when the tip of the Mach line (point B in figure 10*a*) crossed the velocity measurement position M. At 50 µs, the sliding tip B was to the left of the measurement position (figure 10*b*), signifying that the sliding had already started. Point B was travelling at a supershear speed of $1932\ \mathrm{m\,s^{-1}} = 1.55\,C_2^{\mathrm{H}}$. Figure 11*a* shows that at around 60 µs the horizontal velocity reached its maximum value and the sliding continued for the rest of the recording time with no large variations in the sliding tip speed.

It is interesting to follow the evolution of the vertical velocity in figure 11*a*, and especially the evolution of the vertical displacement depicted in figure 11*b*.

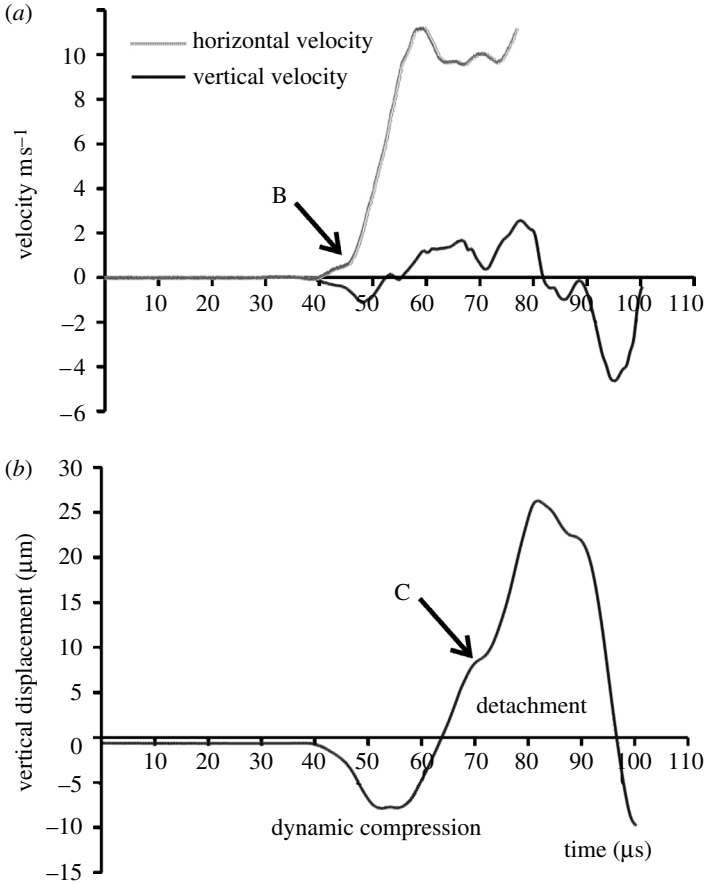

Figure 11. (*a*) Histories of the horizontal and the vertical components of the in-plane particle velocity measured on the Homalite plate, 70 mm from its impact side. The sliding initiated at B. The confining stress was 5 MPa and the impact speed was 22 m s^{-1}. (*b*) History of the vertical displacement.

It is noted that the vertical displacement was obtained from the vertical velocity history by numerical integration. At the start, the specimen was subjected to a uniform external compression of 5 MPa. A very simple one-dimensional calculation showed that the vertical displacement of point N from the initial uncompressed position was less than 1 μm. The impact wave created a dynamic (inertial) compression, which added to the static compression and the displacement became more negative. However, after 55 μs, the vertical velocity became positive, which means that point N was moving upward, approaching the initial uncompressed position. At approximately 65 μs, the displacement became positive, signifying the initiation of the detachment of the Homalite plate from the steel plate. At approximately 95 μs, the opening closed and sliding continued again under compression. Looking at the photoelastic images in figure 10, we see that at 65 μs a fringe structure (shown by arrow C) approached the measurement position. At 70 μs this structure arrived at N, when an interface opening started. At 100 μs (see figure 10*f*), when the opening had closed, the fringe structure had

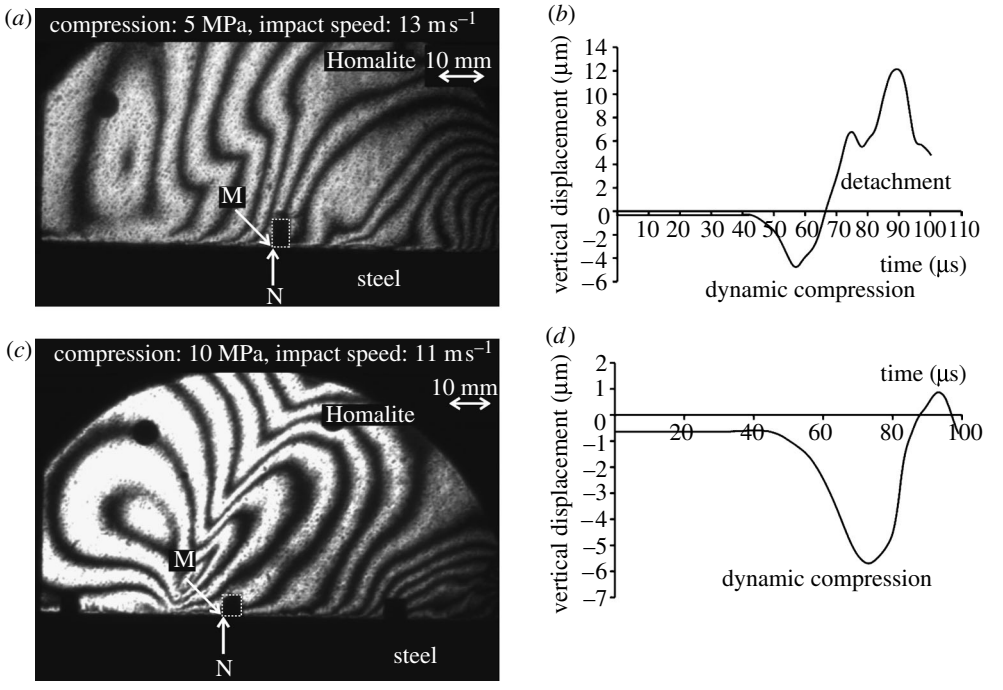

Figure 12. Representative isochromatic fringe patterns and corresponding vertical displacement histories measured on the Homalite plate, 70 mm from its impact side.

departed from N. The propagation speed of this fringe pattern was $1260\,\mathrm{m\,s^{-1}} = 1.0\,C_2^{\mathrm{H}}$, the shear wave speed of Homalite. The data show that the above fringe structure represents a wrinkle-like pulse travelling along the interface. The obtained speed is also consistent with theoretical predictions. The wrinkle-like pulse (detachment wave) had been predicted theoretically by Comninou & Dundurs (1977) and Weertman (1980) and numerically by Andrews & Ben-Zion (1997). However, this is the first observation of a wrinkle-like pulse at high strain rate experiments on elastic bimaterials. Optical evidence of wrinkle-like pulses travelling along interfaces of similar-material plates have also been recorded (see Lykotrafitis & Rosakis in press). Anooshehpoor & Brune (1999) have found similar wrinkle-like pulses in sliding experiments involving very slow wave speed materials such as foam rubber. The above-mentioned fringe structure was very robust. It appeared in all of our experiments conducted at high impact speeds and low compressive loads, and was always connected to a local opening. We mention that the wrinkle-like pulse was not present in the first experiment, because the impact speed was not high enough to trigger detachment. Finally, we note that the whole area from point B to point C in figure 10*a* was sliding under compression.

As the impact speed decreased, we expect that the wrinkle-like pulse will create smaller vertical separation. In figure 12*a*, a photoelastic image shows the fringe pattern at a specific time in the case of a projectile speed of $13\,\mathrm{m\,s^{-1}}$ and a confining pressure of 5 MPa. Although the fringe density is lower than that in figure 10, the eye-like structure and the following Mach line are clearly visible. The supershear speed of the sliding tip was approximately $1833\,\mathrm{m\,s^{-1}} = 1.47\,C_2^{\mathrm{H}}$.

A broad fringe structure located just behind the measurement point M signifies the wrinkle-like pulse. It is less visible than that in figure 10, where the impact speed was higher. Its propagation speed was $1261\,\mathrm{m\,s^{-1}} = 1.0\,C_2^{\mathrm{H}}$. The time evolution of the vertical displacement at the measurement position is displayed in figure 12*b*. As in the case of the lower impact speed, the loading wave generates compression and a decompression period follows later. The maximum opening was approximately 12 μm, almost half of the opening produced in the case of $22\,\mathrm{m\,s^{-1}}$. Experiments at lower impact speeds than $13\,\mathrm{m\,s^{-1}}$ and at the same external pressure show reduced decompression produced by the wrinkle-like pulse. By increasing the confining stress, the same effect was observed: the decompression decreased. Figure 12*c* shows a snapshot of the isochromatic fringes generated by an impact speed of $11\,\mathrm{m\,s^{-1}}$ while the external applied stress was 10 MPa. It is noted that no visual sign of a wrinkle-like pulse appears in the full field photoelastic images. The history of vertical displacement (figure 12*d*) shows that after the initial dynamic compression caused by the impact loading, the decompression was not enough to produce a significant positive displacement. Thus, in this case, there was not any wrinkle-like pulse propagated along the interface, consistent with the fact that no fringe structure characteristic of the wrinkle-like pulse appears in the corresponding photoelastic image. We finally note that the wrinkle-like pulse did not appear in some of the experiments presented in the previous section as well (see figures 5 and 7*a*), because the impact speed was again not high enough to produce detachment.

(*d*) *Frictional sliding induced by high impact speeds*

In the experimental results, we have presented up to this point, the impact speeds were low, less than $22\,\mathrm{m\,s^{-1}}$. In this section, dynamic sliding initiated by impact speeds on the order of $50\,\mathrm{m\,s^{-1}}$ will be investigated. Only photoelasticity will be employed here, since the resulting maximum particle velocities from the impact loading were well beyond $10\,\mathrm{m\,s^{-1}}$, which is the limit of the velocimeter.

Figure 13*b* displays an instantaneous isochromatic fringe pattern generated by an impact speed of $52\,\mathrm{m\,s^{-1}}$, at a uniform confining stress of 10 MPa. It is observed that while the basic characteristic features, which appeared in cases at lower impact speeds and at the same confining stress (see, e.g. figure 5*a*) are also present here, new features emerge in the picture. An eye-like fringe pattern travelling behind the P-wave front (F) emanated from the interface. A head-wave originating from point A ahead of the P-wave front crossed the eye-like fringe formation. The inclination of the Mach line shows that the head wave was created by a disturbance moving along the interface at a supersonic speed (with respect to Homalite) of $2813\,\mathrm{m\,s^{-1}} = 2.25\,C_2^{\mathrm{H}} = 1.1\,C_1^{\mathrm{H}} = 1.3\,C_{1\sigma}^{\mathrm{H}}$. We note at this point that owing to the high impact speed, the head wave was intensified and thus became clearly visible. Figure 13*b* answers positively any scepticism regarding the existence of such a wave based on the poor definition of the Mach line in previous cases at lower impact speeds. Figure 14*a* depicts the computed speeds of the head wave at various frames, using the relation $V = C_2^{\mathrm{H}}/\sin\theta$, and the obtained average value. A second Mach line, behind the eye-like fringe structure, emanates from the supershear sliding tip B. The sliding propagation speed of $2563\,\mathrm{m\,s^{-1}} = 2.0\,C_2^{\mathrm{H}} = 1.0\,C_1^{\mathrm{H}} = 0.79\,C_2^{\mathrm{S}}$ was obtained from the inclination angle of the well-defined Mach line (figure 14*a*). Both Mach lines are highlighted in

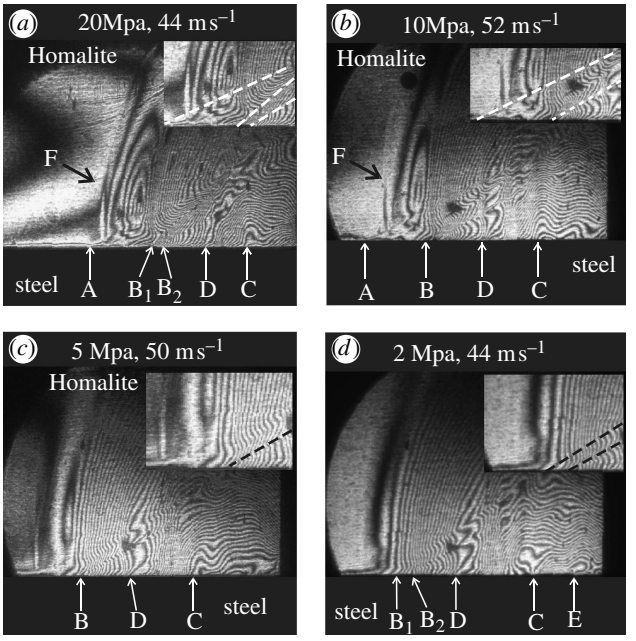

Figure 13. Representative isochromatic fringe patterns from two different experiments at high impact speeds. The specimens were subjected to different confining stresses. Arrow A indicates the position of the disturbance which created the head wave. The arrows B, C, D and F indicate the positions of the rupture tip, of the wrinkle-like pulse, of the fast interface disturbance and of the P-wave front, respectively. The arrow E indicates a second wrinkle-like pulse. The arrow B_1 and B_2 indicate the positions of the sliding tips which are the origin of a transient double shock.

the insert of figure 13*b*. Comparable experimental and numerical results, regarding the speed of the sliding tip, have been obtained by Coker *et al.* (2003) in the case of a dynamic crack growth along a composite-Homalite cohesive interface induced by an impact loading similar to that used in the present experiment. Two robust fringe structures appear behind the rupture tip (points C and D in figure 13*b*). Following their position at different recorded photoelastic frames, their speeds were obtained through a linear interpolation. Figure 14*b* shows the positions of points C and D in various frames and the computed corresponding propagation speeds. The speed of point D was $2294\,\mathrm{m\,s^{-1}} = 1.84\,C_2^{\mathrm{H}} = 0.71\,C_2^{\mathrm{S}}$. The fringe structure at point D could perhaps be linked to a theoretically predicted disturbance by Ranjith & Rice (2001), who studied the slip dynamics at an interface between dissimilar materials. In the case of a large contrast bimaterial system (steel–PMMA), they traced a disturbance travelling along the interface at a speed of $1.84\,C_2^{\mathrm{PMMA}}$, similar to the speed of the disturbance that appeared in our experiments. PMMA is a brittle polymer (polymethylmethacrylate) otherwise known as plexiglas. We also note that the disturbance at point D was robust and appeared in a persistent manner at high impact speed experiments. Its appearance becomes more pronounced as the confining stress decreases (see figure 13*c*,*d*). Point C was travelling at a speed of $1199\,\mathrm{m\,s^{-1}} = 0.96\,C_2^{\mathrm{H}}$ and we conclude that the corresponding fringe structure reflected the propagation of a wrinkle-like pulse along the interface, consistent with the results obtained at lower impact speeds.

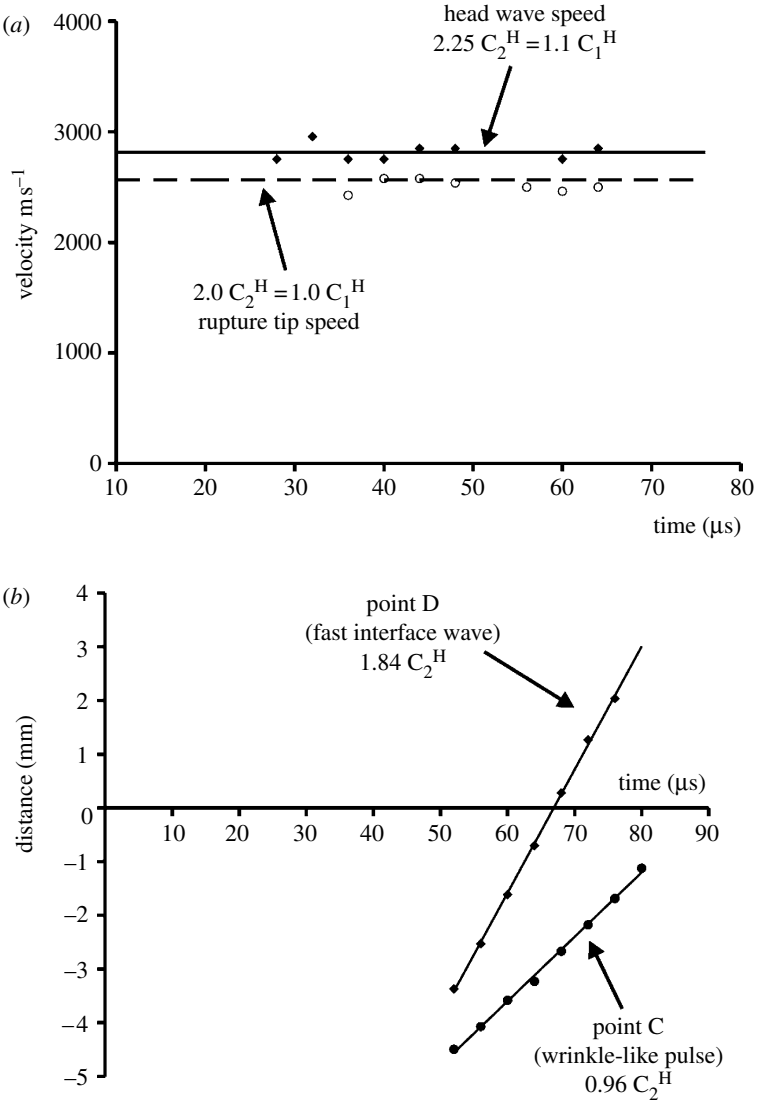

Figure 14. (*a*) Sliding tip speeds and head wave speeds at different frames measured using the Mach angle. (*b*) Positions of the wrinkle-like pulse and the fast interface disturbance as a function of time. The static pre-stress was 10 MPa and the impact speed was $52\,\mathrm{m\,s^{-1}}$.

At a compression of 20 MPa and at an impact speed of $44\,\mathrm{m\,s^{-1}}$, the same basic features as above arose with the eye-like fringe structure widened (figure 13*a*). A remarkable difference is that in this case two sliding tips (B_1 and B_2) appeared. They travelled at different speeds and they formed an unstable supershear sliding zone, which shrunk with time, as the speed of point B_2 was $2357 = 1.89C_2^{\mathrm{H}}$, higher than the speed of B_1, which was $1854 = 1.48C_2^{\mathrm{H}}$. Because both speeds were supershear, a transient double shock was formed. The disturbance at A, ahead of the P-wave front, was travelling at $2851 = 2.28C_2^{\mathrm{H}}$ again creating a head wave, which crossed the eye-like fringe formation. Behind the unstable segment B_1B_2, both the fast disturbance at D and the wrinkle-like

pulse were present. The wrinkle-like pulse (point C) was travelling at $1237 = 0.99C_2^H$. The fast disturbance D was transient and we were not able to obtain its propagation speed. The insert in figure 13*a* highlights the head wave and the double Mach lines.

As the confining stress was decreased to 5 MPa, the eye-like fringe structure shrank (figure 13*c*) and it almost completely disappeared at 2 MPa (figure 13*d*). In figure 13*c*, the Mach line corresponds to a rupture tip velocity of $2545 = 2.0C_2^H$. The fast disturbance at D was travelling at $2178 = 1.74C_2^H$ while the speed of the wrinkle-like pulse at C was $1234 = 0.99C_2^H$. In the case displayed in figure 13*d*, the confining stress was very low at 2 MPa and the impact speed was 44 m s^{-1}. An unstable double shock wave was emanating from points B_1 and B_2, which were travelling at speeds of $2039\,\mathrm{m\,s^{-1}} = 1.63C_2^H$ and $2039\,\mathrm{m\,s^{-1}} = 1.63C_2^H$, respectively. The fast and slow (wrinkle-like) disturbances also appeared, propagating at speeds of $2039\,\mathrm{m\,s^{-1}} = 1.63C_2^H$ and $1151\,\mathrm{m\,s^{-1}} = 0.92C_2^H$, respectively. In addition, another slow interface disturbance appeared at point E. Its speed was $1125\,\mathrm{m\,s^{-1}} = 0.9C_2^H$ and it seems that it is of the wrinkle-like type, since the fringe structure and the propagation speed are similar to the corresponding features of the wrinkle-like pulses. This result, along with results obtained from experiments performed at similar conditions, shows that as the confining pressure decreased, two or more wrinkle-like pulses propagated along the interface, since a local opening occurred more easily.

(*e*) *Study of the speeds of the various features propagating along the bimaterial interface*

The propagation speeds for the head wave, the sliding tip, the fast interface disturbance and for the wrinkle-like pulse for various impact speeds and for different confining stresses are displayed in figure 15. As the impact speed increased, the propagation speed of the sliding tip also increased, approaching the P-wave speed of Homalite (figure 15*b*). The rupture tip speeds were supershear with respect to Homalite for all the performed experiments. Figure 15*a* shows that the head wave speed, which was consistently lower than the shear wave of steel but higher than the P-wave speed of Homalite, did not depend on the impact speed. The same is true for the wrinkle-like pulse. Its speed was, within an experimental error, between the Rayleigh wave speed and the shear wave speed of Homalite (figure 15*d*), consistent with the theoretical values obtained by Comninou & Dundurs (1977). The speed of the fast interface disturbance was also not dependent on the impact speed (figure 15*c*). We note, however, that this disturbance, unlike the previous features, was transient at confining stresses of 10 and 20 MPa, and only with lower static pressures did it have a persistent appearance and a robust form.

5. Sliding induced by impact shear loading applied on the steel plate of the bimaterial specimen

In this section, dynamic sliding initiated by impact loading applied on the steel plate is investigated. Figure 16*a* shows the isochromatic fringe pattern developed in the Homalite plate at a selected time with an impact speed of 17 m s^{-1} and

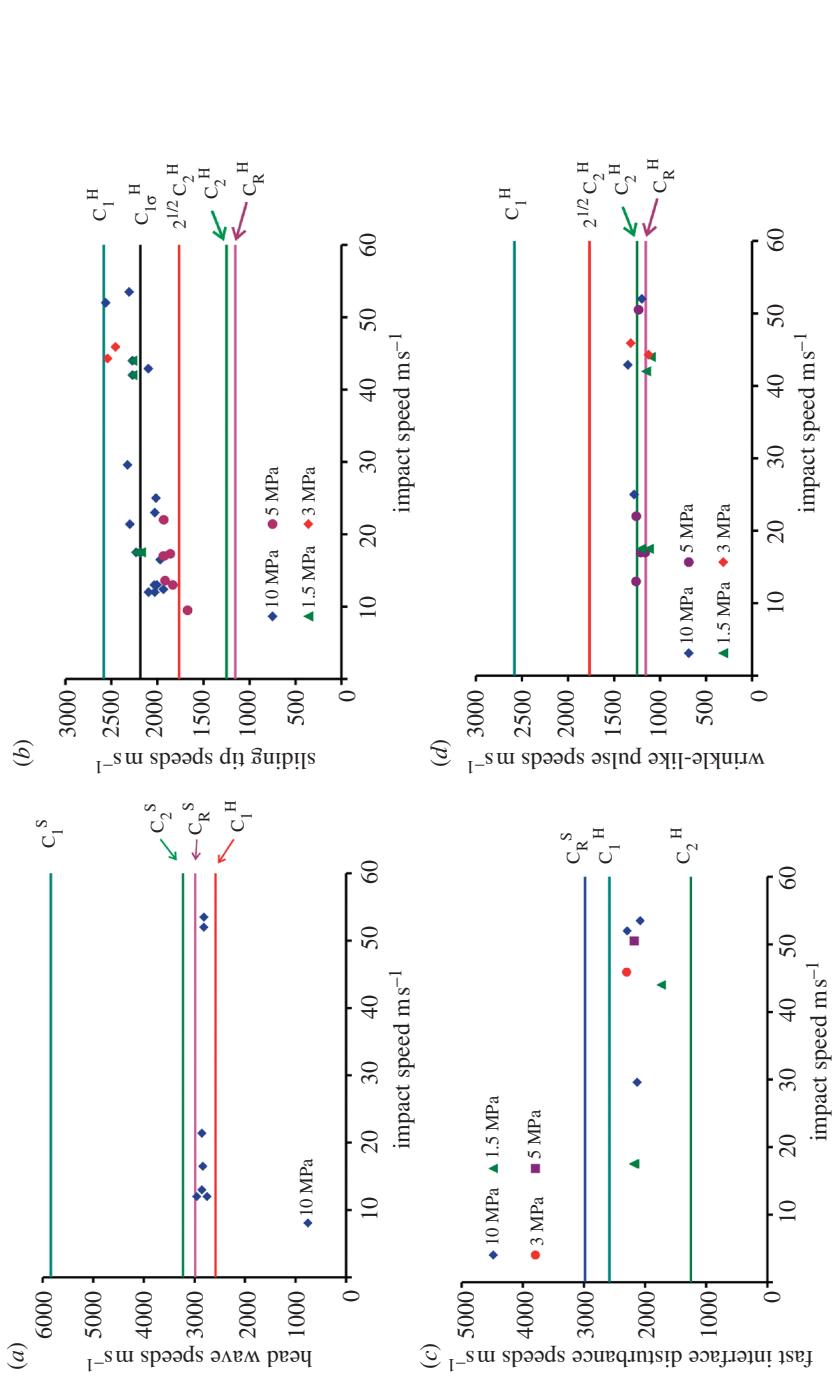

Figure 15. (*a*) The head wave speed is independent of the impact speed. (*b*) Variation of the sliding tip speed with the impact speed for various confining stresses. (*c*) The speed of the fast interface disturbance did not depend on the impact speed or on the confining stress. (*d*) The wrinkle-like pulse speed remained between the Rayleigh wave speed and the shear wave speed of Homalite-100, independent of the impact speed and the confining stress.

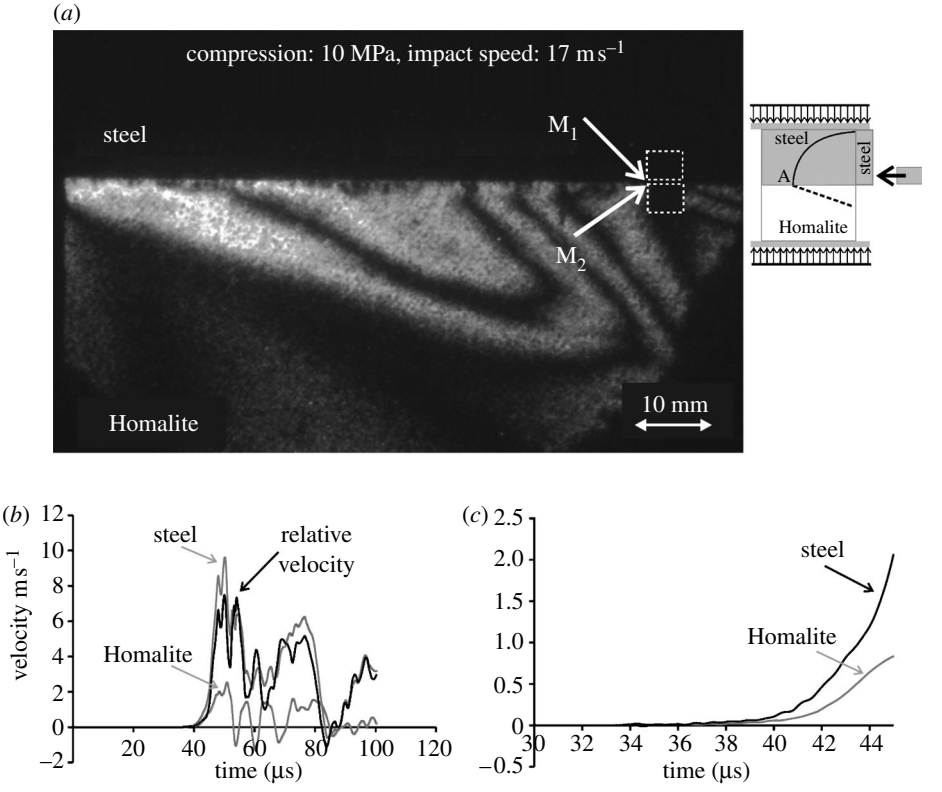

Figure 16. (*a*) Representative isochromatic fringe pattern from an experiment of sliding propagation initiated by impact on the steel plate. (*b*) Histories of the horizontal in-plane velocities and of the relative velocity, measured at two adjacent points M_1 and M_2, 30 mm from the impact side of the Homalite plate. (*c*) Detail of the velocities histories diagram.

a confining stress of 10 MPa. The formation of a shear Mach line shows that a disturbance was travelling along the bimaterial interface at a speed higher than the shear wave speed of Homalite. The inclination angle of the Mach line was approximately 18°, which corresponds to a $4042\,\mathrm{m\,s^{-1}} = 1.25\,C_2^{\mathrm{S}} = 0.7\,C_1^{\mathrm{S}}$ propagation speed of the disturbance. This result means that the disturbance follows closely the P-wave front in the steel plate. For more information, however, we have to resort to velocimetry since photoelasticity is not very helpful given that the photoelastic images do not have enough structure. This happens because the dynamic vertical compressive stress was very low, since the Young modulus of steel is large and thus the Poisson effect was very limited during sliding. Figure 16*b* depicts the evolution with time of the in-plane horizontal velocities of two points M_1 and M_2 (across the interface), which belonged to steel and Homalite plates, respectively. The distance of M_1 and M_2 from the impact side of the steel plate was 30 mm and their distance from the interface was less than 250 μm. The velocity of point M_1 on the steel plate was higher that the velocity of point M_2 on the Homalite plate, despite the fact that steel is much a stiffer material than Homalite. This shows that the energy transfer from the steel plate to the Homalite plate was not efficient. The Poisson

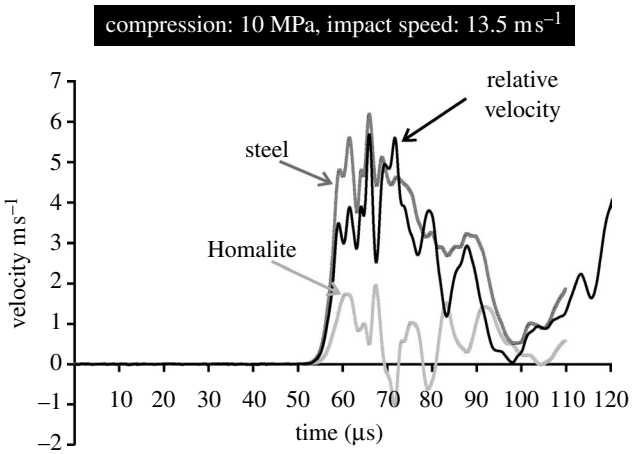

Figure 17. Histories of the horizontal in-plane velocities and of the relative velocity, measured at two adjacent points across the interface, 30 mm from the impact side of the Homalite plate.

effect, as we have already mentioned above, was minor and the dynamic (inertial) compression applied to the Homalite plate was low. Consequently, the frictional resistance was also low, and the local sliding initiated almost immediately with the arrival of the P-wave front there, without any significant elastic deformation of the Homalite surface. This is clear from figure 16*c*, where the velocity history of points M_1 and M_2 at the first microseconds of the sliding initiation is depicted. The velocity of point M_1 on the steel plate started increasing at approximately 37 μs because of the horizontal compression applied from the dilatational wave. Almost immediately, point M_2 (on the Homalite plate surface) started moving, dragged by the motion in the steel plate because of friction. At 40 μs the relative velocity increased rapidly and sliding started (figure 16*b*). This shows that elastic deformation happened at the very first 3 μs after the dilatational wave arrival at M_1. The above result obtained through velocimetry agrees with the result obtained via photoelasticity (that a supershear disturbance, with respect to Homalite, was propagating along the interface just behind the P-wave front in steel) and makes clear that the disturbance was the sliding tip. It also agrees with both the experimental and numerical results obtained by Coker *et al.* (2003). We note that the process of sliding initiation was different in the case, where the Homalite plate was impacted. For example, figure 6*b* shows that for approximately 24 μs points M_1 and M_2 were travelling together, since merely elastic deformation occurred during this period. Only after 24 μs elapsed did the sliding start.

Figure 17 displays the history of the in-plane horizontal velocities of points M_1 and M_2, belonging to steel and Homalite plates, respectively. The external confining stress was 10 MPa and the impact speed was 13.5 m s^{-1}. The horizontal distance of points M_1 and M_2 from the impact side of the Homalite plate was again 30 mm. The sliding initiation procedure was very similar to that depicted in figure 16*b*. We also note that the duration of the initial sliding period was approximately 43 μs (from 55 to 98 μs), the same for both cases. The only difference is that the maximum horizontal velocity of M_1 was lower than in

the previous case, since the impact speed was lower here. The velocity of point M_2 in Homalite plate was also lower in figure 17 than in figure 16.

We finally note that in all the performed experiments the duration of local sliding was long, and we conclude that rupture occurred in a crack-like mode.

6. Concluding remarks

A new technique has been developed to record the evolution of the in-plane components of the particle velocity in real time. The combination of velocimetry with the full-field technique of dynamic photoelasticity was proven to be a very powerful tool in the study of dynamic frictional sliding along incoherent interfaces.

The experiments involved bimaterial specimens consisting of Homalite-100 and steel plates held together by uniform compressive stress and subjected to impact shear loading. When the impact loading was applied to the Homalite plate, the following effects were captured:

(i) The interaction between the impact wave and the pre-existing static stress field caused a relatively broad loading wave that emanated from the interface.
(ii) A disturbance, travelling along the interface at a speed close to the Rayleigh wave speed of steel, generated a Mach line that crossed the P-wave front and the eye-like fringe pattern. Data recorded by the velocimeter showed that this disturbance affected the relative velocity, but did not cause sliding.
(iii) The velocimeter revealed that the sliding initiated behind the eye-like fringe structure. A shear Mach line was visible in the photoelastic images, indicating that the sliding was supershear with respect to the shear wave speed of Homalite.
(iv) The sliding occurred in a crack-like mode.
(v) A fast interface disturbance was captured propagating behind the rupture tip at high impact speeds.
(vi) A self-sustaining wrinkle-like pulse propagating along the bimaterial interface was observed. It caused a local detachment between the two plates that was travelling at a speed close to the Rayleigh wave speed of Homalite. It is expected that the wrinkle-like pulse might play an important role in the failure mechanism of bimaterial structures subjected to impact shear loading.

When the impact loading was applied to the steel plate, then velocimetry was the only source of information. Sliding at a point on the interface started almost immediately with the arrival of the P-wave front there and it occurred in a crack-like mode in all the performed experiments.

The authors gratefully acknowledge the support of the Office of Naval Research through grant N00014-03-1-0435 and the Department of Energy through grant DE-FG52-06NA26209. Many helpful discussions with Professors A. Needleman and D. Coker are gratefully acknowledged.

References

Achenbach, J. D. & Epstein, H. I. 1967 Dynamic interaction of a layer and a half-space. *J. Eng. Mech.* **5**, 27–42.

Adams, G. 1995 Self-excited oscillations of two elastic half-spaces sliding with a constant coefficient of friction. *J. Appl. Mech.* **62**, 867–872.

Andrews, D. J. 1976 Rupture velocity of plain strain shear cracks. *J. Geophys. Res.* **81**, 5679–5687.

Andrews, D. J. & Ben-Zion, Y. 1997 Wrinkle-like slip pulse on a fault between different materials. *J. Geophys. Res.* **102**, 553–571. (doi:10.1029/96JB02856)

Andrews, D. J. & Harris, R. A. 2005 The wrinkle-like slip pulse is not important in earthquake dynamics. *Geophys. Res. Lett.* **32**, L23 303. (doi:10.1029/2005GL023996)

Anooshehpoor, A. & Brune, J. N. 1999 Wrinkle-like Weertman pulse at the interface between two blocks of foam rubber with different velocities. *Geophys. Res. Lett.* **23**, 2025–2028. (doi:10.1029/1999GL900397)

Archuletta, R. J. 1984 A faulting model for the 1979 Imperial Valley earthquake. *J. Geophys. Res.* **89**, 4559–4585.

Ben-Zion, Y. & Andrews, D. J. 1998 Properties and implications of dynamic rupture along a material interface. *Bull. Seismol. Soc. Am.* **88**, 1085–1094.

Broberg, K. B. 1999 *Cracks and fracture*. London: Academic Press.

Cochard, A. & Rice, J. 2000 Fault rupture between dissimilar materials: ill-posedness, regularization, and slip-pulse response. *J. Geophys. Res.* **105**, 25 891–25 907. (doi:10.1029/2000JB900230)

Coker, D., Rosakis, A. J. & Needleman, A. 2003 Dynamic crack growth along a polymer composite-Homalite interface. *J. Mech. Phys. Solids* **51**, 425–460. (doi:10.1016/S0022-5096(02)00082-0)

Coker, D., Lykotrafitis, G., Needleman, A. & Rosakis, A. J. 2005 Frictional sliding modes along an interface between identical elastic plates subject to shear impact loading. *J. Mech. Phys. Solids* **53**, 884–922. (doi:10.1016/j.jmps.2004.11.003)

Comninou, M. & Dundurs, J. 1977 Elastic interface waves involving separation. *ASME J. Appl. Mech.* **44**, 222–226.

Day, S. M. 1982 Three-dimensional simulation of spontaneous rupture: the effect of non-uniform prestress. *Bull. Seismol. Soc. Am.* **50**, 643–668.

Dieterich, J. H. 1979 Modeling of rock friction 1. Experimental results and constitutive equations. *J. Geophys. Res.* **84**, 2161–2168.

Freund, L. B. 1990 *Dynamic fracture mechanics*. Cambridge: Cambridge University Press.

Harris, R. A. & Day, S. M. 1997 Effects of a low-velocity zone on a dynamic rupture. *Bull. Seismol. Soc. Am.* **87**, 1267–1280.

Harris, R. A. & Day, S. M. 2005 Material contrast does not predict earthquake rupture propagation direction. *Geophys. Res. Lett.* **32**, L23 301. (doi:10.1029/2005GL023941)

Heaton, T. H. 1990 Evidence for and implications of self-healing pulses of slip in earthquake rupture. *Phys. Earth Planet. Int.* **64**, 1–20. (doi:10.1016/0031-9201(90)90002-F)

Kavaturu, M., Shukla, A. & Rosakis, A. J. 1998 Intersonic crack propagation and interfaces: experimental observations and analysis. *Exp. Mech.* **38**, 218–225. (doi:10.1007/BF02325746)

Lambros, J. & Rosakis, A. J. 1995 Shear dominated transonic interfacial crack growth in a bimaterial-I. Experimental observations. *J. Mech. Phys. Solids* **43**, 169–188. (doi:10.1016/0022-5096(94)00071-C)

Linker, M. F. & Dieterich, J. H. 1992 Effects of variable normal stress on rock friction: observations and constitutive equations. *J. Geophys. Res.* **97**, 4923–4940.

Liu, C., Lambros, J. & Rosakis, A. J. 1993 Highly transient elastodynamic crack growth in a bimaterial interface: higher order asymptotic analysis and optical experiments. *J. Mech. Phys. Solids* **41**, 1857–1954.

Lykotrafitis, G. & Rosakis, A. J. In press. Sliding along frictionally-held incoherent interfaces in homogeneous systems under dynamic shear loading. *Int. J. Fract.*

Lykotrafitis, G., Rosakis, A. J. & Ravichandran, G. 2006 Particle velocimetry and photoelasticity applied to the study of dynamic sliding along frictionally-held bimaterial interfaces: techniques and feasibility. *Exp. Mech.* **46**, 205–216. (doi:10.1007/S11340-006-6418-4)

Persson, B. N. J. 2000 *Sliding friction physical principles and applications*. Berlin: Springer.

Prakash, V. 1998 Frictional response of sliding interfaces subjected to time varying normal pressures. *J. Tribol. ASME* **120**, 97–102.

Prakash, V. & Clifton, R. J. 1993 Pressure-shear plate impact measurement of dynamic friction for high speed machining applications. *Proc. Int. Cong. on Experimental Mechanics, Society of Experimental Mechanics, Bechtel, CT*, pp. 556–564.

Ranjith, K. & Rice, J. R. 2001 Slip dynamics at an interface between dissimilar materials. *J. Mech. Phys. Solids* **49**, 341–361. (doi:10.1016/S0022-5096(00)00029-6)

Renardy, M. 1992 Ill-posedness at the boundary for elastic solids sliding under Coulomb friction. *J. Elasticity* **27**, 281–287.

Rice, J. R. 2001 Mechanics for a new millennium. In *Proc. Int. Cong. of Theoretical and Applied Mechanics, 2000, Chicago* (eds. H. Aref & J. W. Philips), pp. 1–23. Dordrecht: Kluwer Academic Publishers.

Rice, J. R. & Ruina, A. L. 1983 Stability of frictional sliding. *J. Appl. Mech.* **50**, 343–349.

Rice, J. R., Lapusta, N. & Ranjith, K. 2001 Rate and state dependent friction and the stability of sliding between elastically deformable solids. *J. Mech. Phys. Solids* **49**, 1865–1898. (doi:10.1016/S0022-5096(01)00042-4)

Rosakis, A. J. 2002 Intersonic shear cracks and fault ruptures. *Adv. Phys.* **51**, 1189–1257. (doi:10.1080/00018730210122328)

Rosakis, A. J., Samudrala, O., Singh, R. P. & Shuckla, A. 1998 Intersonic crack propagation in bimaterial systems. *J. Mech. Phys. Solids* **46**, 1789–1813. (doi:10.1016/S0022-5096(98)00036-2)

Ruina, A. L. 1983 Slip instability and state variable friction laws. *J. Geophys. Res.* **88**, 10 359–10 370.

Samudrala, O. & Rosakis, A. J. 2003 Effect of loading and geometry on the subsonic/intersonic transition of bimaterial interface crack. *Eng. Fract. Mech.* **70**, 309–337. (doi:10.1016/S0013-7944(02)00025-5)

Samudrala, O., Huang, Y. & Rosakis, A. J. 2002 Subsonic and intersonic mode II crack propagation with a rate-dependent cohesive zone. *J. Mech. Phys. Solids* **50**, 1231–1268. (doi:10.1016/S0022-5096(01)00129-6)

Schallamach, A. 1971 How does rubber slide? *Wear* **17**, 301–312. (doi:10.1016/0043-1648(71)90033-0)

Singh, P. R. & Shukla, A. 1996 Subsonic and transonic crack growth along a bimaterial interface. *ASME J. Appl. Mech.* **63**, 919–924.

Tippur, H. V. & Rosakis, A. J. 1991 Quasi-static and dynamic crack growth along bimaterial interfaces: a note on crack-tip field measurements using coherent gradient sensing. *Exp. Mech.* **31**, 243–251. (doi:10.1007/BF02326067)

Weertman, J. 1980 Unstable slippage across a fault that separates elastic media of different elastic constants. *J. Geophys. Res.* **85**, 1455–1461.